nature cell biology

LETTERS

https://doi.org/10.1038/s41556-020-0564-2

Lipid peroxidation regulates long-range wound detection through 5-lipoxygenase in zebrafish

Anushka Katikaneni[1,4], Mark Jelcic[1,2,4], Gary F. Gerlach[3], Yanan Ma[1], Michael Overholtzer[1] and Philipp Niethammer[1]✉

Rapid wound detection by distant leukocytes is essential for antimicrobial defence and post-infection survival[1]. The reactive oxygen species hydrogen peroxide and the polyunsaturated fatty acid arachidonic acid are among the earliest known mediators of this process[2–4]. It is unknown whether or how these highly conserved cues collaborate to achieve wound detection over distances of several hundreds of micrometres within a few minutes. To investigate this, we locally applied arachidonic acid and skin-permeable peroxide by micropipette perfusion to unwounded zebrafish tail fins. As in wounds, arachidonic acid rapidly attracted leukocytes through dual oxidase (Duox) and 5-lipoxygenase (Alox5a). Peroxide promoted chemotaxis to arachidonic acid without being chemotactic on its own. Intravital biosensor imaging showed that wound peroxide and arachidonic acid converged on half-millimetre-long lipid peroxidation gradients that promoted leukocyte attraction. Our data suggest that lipid peroxidation functions as a spatial redox relay that enables long-range detection of early wound cues by immune cells, outlining a beneficial role for this otherwise toxic process.

Hydrogen peroxide (H_2O_2) is a relatively stable reactive oxygen species (ROS) produced by NADPH oxidase or mitochondria in cells. At wounds, it rapidly forms concentration gradients proposed to provide paracrine regulation of wound healing, inflammation and regeneration throughout phylae[2,5]. H_2O_2 can bias immune cell motility in vitro[3,6] and promote leukocyte recruitment to injury sites, at least in part through redox activation of Lyn[3,7]. However, quantitative analysis of wound peroxide gradients in live zebrafish suggests that these patterns do not reach far enough to directly alter redox signalling in cells farther than ~30 µm from the wound margin[8]. Notably, in the same model, leukocytes are rapidly summoned from distances of up to ~300 µm. Thus, some relay mechanism must exist that extends the chemotactic signalling range of the wound peroxide gradient by roughly an order of magnitude.

Together with peroxide, arachidonic acid (AA) is locally released at wounds by a mechanosensitive phospholipase ($cPLA_2$) in response to calcium signals and nuclear envelope stretch[4,9]. Whereas conventional chemotaxis receptors for peroxide remain elusive, AA fuels the eicosanoid cascade—a metabolic pathway that oxidizes AA into potent lipid chemoattractants, such as the G protein-coupled receptor ligands leukotriene B_4 and 5-oxo-eicosatetraenoic acid (5-oxoETE). Bathing wounded zebrafish larvae in exogenous AA, when wound-induced AA release is osmotically prevented, reconstitutes rapid leukocyte recruitment to injury sites[4]. Yet, as for wound peroxide, it is unclear whether AA just amplifies chemotaxis to other wound signals (for example, by promoting leukotriene-mediated relay signalling between leukocytes[10]) or whether it can act as a primary wound chemoattractant itself.

Zebrafish larvae are a powerful model for innate immune responses[11]. Their tail fin tissue is not vascularized; hence, interstitial and vascular damage detection mechanisms can be studied separately. In healthy, unwounded tail fins, neutrophils are largely confined to the caudal haematopoietic region. Thus, fin injury can be applied at a secure distance (100–300 µm) from a leukocyte, minimizing the risk of inadvertently injuring and activating it.

To test whether local AA or peroxide application suffices to attract leukocytes in vivo, we patched a custom-forged, polished micropipette (tip diameter: ~10–20 µm) filled with AA onto unwounded zebrafish tail fins using mild, non-damaging suction applied by a syringe. We then monitored rapid leukocyte responses by transmitted light imaging (Fig. 1a and Supplementary Video 1). Native AA is not a leukocyte chemoattractant and intact larval tail fins typically lack interstitial leukocytes that could oxidize AA into leukotrienes. However, AA microperfusion caused massive leukocyte recruitment to the pipette tip at concentrations ≥5 µM. As for a wound, microperfused AA mobilized leukocytes from up to ~300 µm towards the signal source within ~10 min. Different commercial AA preparations gave similar responses (Extended Data Fig. 1a). The number of responsive leukocytes depended on the AA dose: 5 µM AA (Fig. 1b) mobilized about half as many leukocytes as 20 µM (Fig. 1c). These concentrations are within the range of free AA measured in normal or inflamed human skin[12]. After detachment of the pipette, leukocytes immediately returned to the vascular region (Supplementary Video 1), reminiscent of reverse leukocyte migration previously described for zebrafish wounds[13]. Next, we tested whether oxidative stress alone could initiate leukocyte recruitment. At zebrafish wounds, the epithelial NADPH oxidase Duox generates extracellular/luminal H_2O_2 by consuming cytoplasmic NADPH[2]. As H_2O_2 does not penetrate intact larval skin[14], we instead microperfused cumene hydroperoxide (CHP)—a lipophilic peroxide often used to trigger lipid peroxidation. CHP treatment elevated tissue H_2O_2 levels (Extended Data Fig. 1b). Although CHP was not chemotactic on its own, it augmented leukocyte mobilization to AA (Fig. 1b). Conversely, local Duox inhibition by co-perfusion of the flavoprotein inhibitor diphenyleneiodonium chloride (DPI) or global *duox* knockdown with an established antisense morpholino[2,3] suppressed the directional migration or responsiveness of leukocytes, respectively, towards microperfused AA (Fig. 1c, Extended Data Fig. 4 and Supplementary Video 2), as previously observed for wounds[2]. At zebrafish wounds, AA metabolites hence act as

[1]Cell Biology Program, Memorial Sloan Kettering Cancer Center, New York, NY, USA. [2]Louis V. Gerstner Jr. Graduate School of Biomedical Sciences, Memorial Sloan Kettering Cancer Center, New York, NY, USA. [3]Department of Cell Biology and Physiology, School of Medicine, University of North Carolina at Chapel Hill, Chapel Hill, NC, USA. [4]These authors contributed equally: Anushka Katikaneni, Mark Jelcic. ✉e-mail: niethamp@mskcc.org

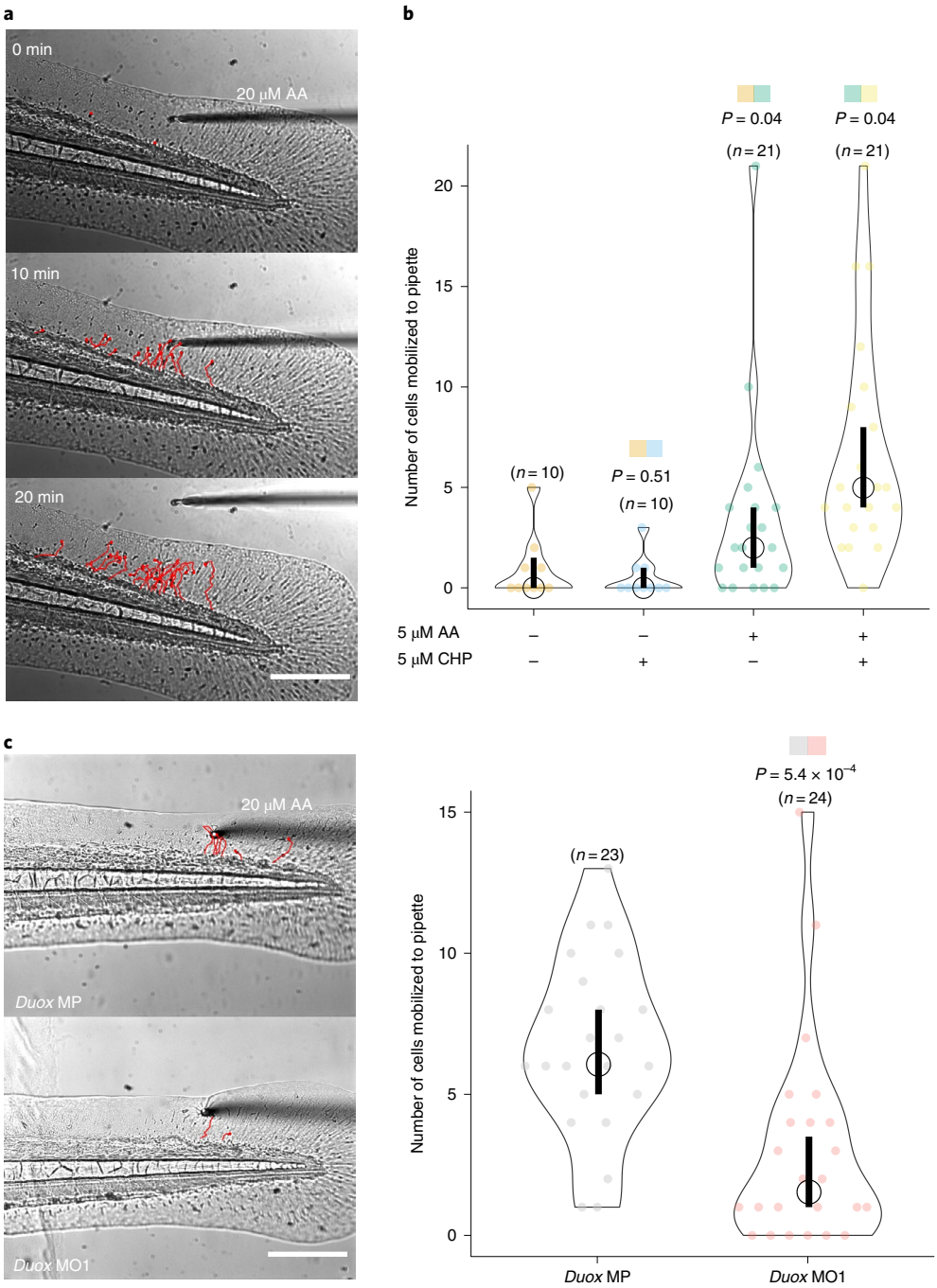

Fig. 1 | Oxidative stress enhances wound detection through the AA pathway. a, Images showing rapid leukocyte migration to 20 μM AA released by a micropipette patched onto an intact (wild-type) larval zebrafish tail fin. Note that leukocytes immediately turned back to the vasculature after the pipette was removed. The red lines show the leukocyte tracks at the indicated times after patching. The results are representative of $n = 3$ biologically independent animal experiments. **b**, Intact fins were perfused with DMSO carrier control, 5 μM CHP, 5 μM AA or 5 μM CHP + 5 μM AA. The violin plot depicts the number of leukocytes per animal mobilized towards the pipette tip within 20 min after patching. Data were aggregated from $n = 10$ (AA^-CHP^-), $n = 10$ (AA^-CHP^+), $n = 21$ (AA^+CHP^-) and $n = 21$ (AA^+CHP^+) biologically independent animal experiments. **c**, Left: representative images of intact tail fins of control (*duox* MP) and *duox* morphant (*duox* MO1) larvae perfused with 20 μM AA, at 20 min after patching. The red lines show the leukocyte tracks. Right: violin plot depicting the number of leukocytes per animal mobilized towards the pipette tip within 20 min after patching. Data were aggregated from $n = 23$ (*duox* MP) and $n = 24$ (*duox* MO1) biologically independent animal experiments. For the violin plots in **b** and **c**: circles represent median values; bars represent 95% confidence intervals; statistical significance was determined by a two-sided, heteroscedastic Student's *t*-test for pairwise comparison of the indicated colour-coded samples; and the values in parentheses show the numbers of different animals. Scale bars, 200 μm (**a** and **c**).

primary, redox-regulated attractants, transcending their known intermediary role in relay chemotaxis and leukocyte swarming.

The synthesis of AA-derived leukocyte chemoattractants is initiated by stereospecific peroxidation of AA by 5-lipoxygenase (Alox5a) and 12-lipoxygenase (Alox12) into 5(*S*)- and 12(*S*)-hydroperoxyeicosatetraenoic acid (HpETE), respectively. Lipoxygenases are intrinsically redox sensitive. Their catalytic iron must be oxidized from ferrous (Fe^{2+}) to ferric (Fe^{3+}) by long-chain

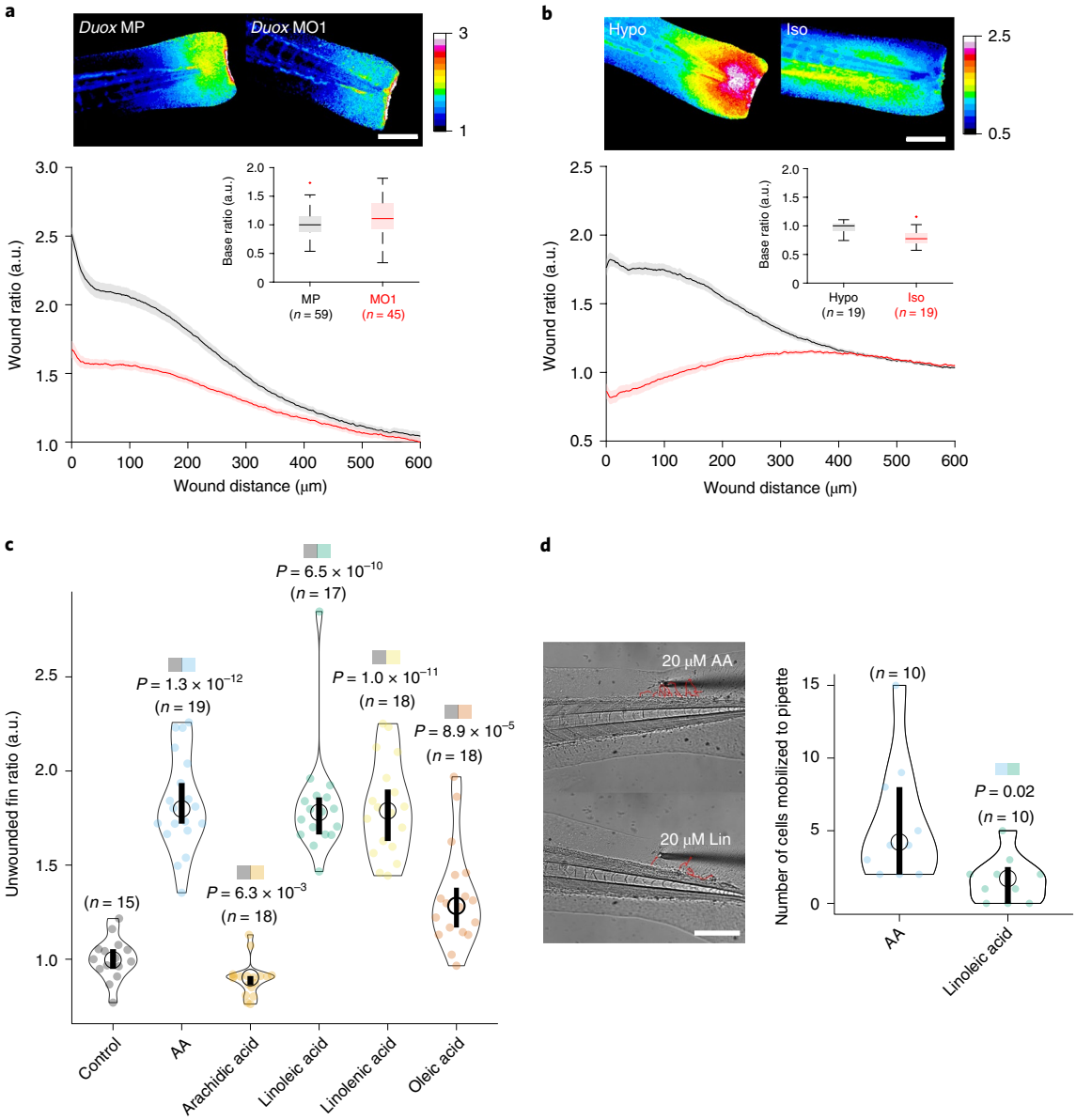

Fig. 2 | Lipid peroxidation gradients integrate oxidative and osmotic wound cues. a,**b**, C11B imaging of control (*duox* MP) and *duox* knockdown (*duox* MO1) zebrafish larvae ~15–30 min after tail fin tip amputation (**a**) and zebrafish larvae ~15–30 min after tail fin tip amputation in hypotonic (Hypo) or isotonic (Iso; that is, Hypo + 135 mM NaCl) bathing solution (**b**). Top: representative C11B ratio images. Bottom: wound ratio (mean C11B ratio normalized to median baseline ratio ± s.e.m.) plotted against wound distance. Inset: box plots of baseline ratios normalized to controls. Central lines represent median values, whereas box edges represent the 25th and 75th percentiles. Whiskers show the most extreme, non-outlier data points. Outliers are shown by a plus sign. Data were aggregated from $n = 59$ (*duox* MP), $n = 45$ (*duox* MO1), $n = 19$ (Hypo) and $n = 19$ (Iso) biologically independent animal experiments. **c**, Violin plot of C11B ratios in unwounded tail fins ~60 min after exposure to 20 μM of the indicated free fatty acids or DMSO carrier control. Data were aggregated from $n = 15$ (control), $n = 19$ (AA), $n = 18$ (arachidic acid), $n = 17$ (linoleic acid), $n = 18$ (linolenic acid) and $n = 18$ (oleic acid) biologically independent animal experiments. **d**, Left: representative images of wild-type tail fins patched with 20 μM AA or linoleic acid at 20 min after patching. The red lines show the leukocyte tracks. Right: violin plot depicting the number of leukocytes per animal mobilized towards the pipette tip within 20 min after patching. Data were aggregated from $n = 10$ (AA) and $n = 10$ (linoleic acid) biologically independent animal experiments. For the violin plots in **c** and **d**: circles represent median values; bars represent 95% confidence intervals; statistical significance was determined by a two-sided, heteroscedastic Student's *t*-test for pairwise comparison of the indicated colour-coded samples; and the values in parentheses show the numbers of different animals. Scale bars, 200 μm (**a**, **b** and **d**).

fatty acid hydroperoxides[15,16], which may be generated by lipoxygenases or non-enzymatic lipid peroxidation. Reduction of H_2O_2 or other organic peroxides by Fe^{2+} provides the radicals (HO• and so on) that start and propel lipid auto-oxidation. Auto-oxidation continuously generates lipid peroxides that, with Fe^{2+}, form new radicals and can activate lipoxygenases. If the process slips out of control, this chain reaction can trigger ferroptotic cell death[17]. Ferroptosis can move through multicellular systems as a wave in vitro and ex vivo[18–20]. Intriguingly, in two of our ~200 micropipette experiments (that is, ~1%), we observed a reminiscent in vivo phenomenon: a rapid wave of tissue deformation (Extended Data Fig. 1c and Supplementary Video 3) surged out from the AA patch

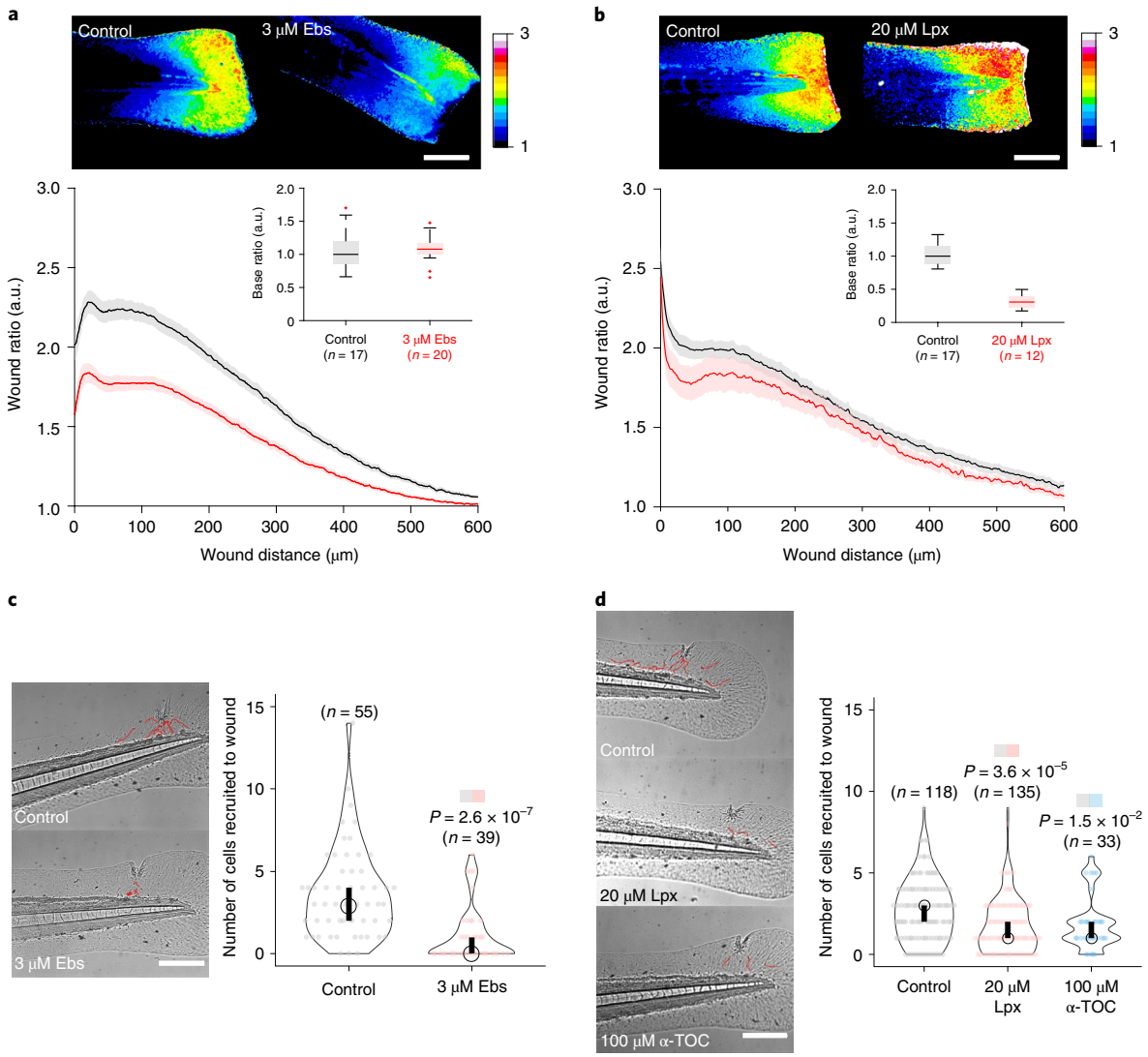

Fig. 3 | Inhibiting lipid peroxidation inhibits wound detection. a,**b**, C11B imaging of control larvae and larvae treated with either the glutathione peroxidase mimetic Ebs (3 μM) (**a**) or the lipid radical scavenger Lpx (20 μM) (**b**) ~15–30 min after tail fin tip amputation. Top: representative C11B ratio images. Bottom: wound ratio (mean C11B ratio normalized to median baseline ratio ± s.e.m.) plotted against wound distance. Inset: box plots of baseline ratios normalized to controls. Central lines represent median values, whereas box edges represent the 25th and 75th percentiles. Whiskers show the most extreme, non-outlier data points. Outliers are shown by a plus sign. Data were aggregated from $n = 17$ (controls in **a** and **b**), $n = 20$ (Ebs) and $n = 12$ (Lpx) biologically independent animal experiments. **c**,**d**, Wounded tail fins were treated with Ebs (3 μM) or DMSO (control) (**c**) or Lpx (20 μM), α-TOC (100 μM) or DMSO (control). Left: representative images of the wounded tail fins at 40 min after injury. The red lines show the leukocyte tracks. Right: violin plots depicting the number of leukocytes per animal recruited to the tail fin wound within 40 min after injury. Data were aggregated from $n = 55$ (control in **c**), $n = 39$ (Ebs), $n = 118$ (control in **d**), $n = 135$ (Lpx) and $n = 33$ (α-TOC) biologically independent animal experiments. For the violin plots in **c** and **d**: circles represent median values; bars represent 95% confidence intervals; statistical significance was determined by a two-sided, heteroscedastic Student's *t*-test for pairwise comparison of the indicated colour-coded samples; and the values in parentheses show the numbers of different animals. Scale bars, 200 μm (**a**–**d**).

site. Its transmitted light features (for example, tissue swelling/collapse and cell opaqueness at patch site) at least seemed consistent with some form of necrotic tissue degeneration. Peroxidation of polyunsaturated fatty acids (PUFAs), such as AA, can drive ferroptosis[21]. It is intriguing to speculate that ferroptotic death waves, such as those reported by Riegman et al.[20] in this issue, can perhaps occur in vivo when antioxidant depletion coincides with the availability of reactive iron and a ferroptotic driver PUFA, such as AA. More work is needed to test this idea.

Interestingly, it was shown that α-tocopherol (α-TOC) depletion of zebrafish larvae promotes formation of the Alox5a metabolite 5-hydroxyeicosatetraenoic acid[22], suggesting that lipid peroxidation regulates this enzyme in vivo. However, the physiological purpose, if any, of redox sensing by Alox5a has remained elusive.

We probed for lipid peroxidation at wounds by ratiometric C11-BODIPY$^{581/591}$ (C11B) imaging. C11B is a fluorescent fatty acid analogue with redox-sensitive double bonds. When those double bonds react with lipid radicals, C11B shifts its fluorescence emission from red to green[23]. Hence, it acts as a fluorescent proxy for radical-mediated PUFA oxidation during lipid peroxidation. Its ratiometric readout allows normalization of sensor signals to the local sensor concentration. We imaged lipid peroxidation in live larvae ~15–30 min after tail fin tip amputation (that is, when the wound-induced H_2O_2 gradient was at peak amplitude[2,8]). For better

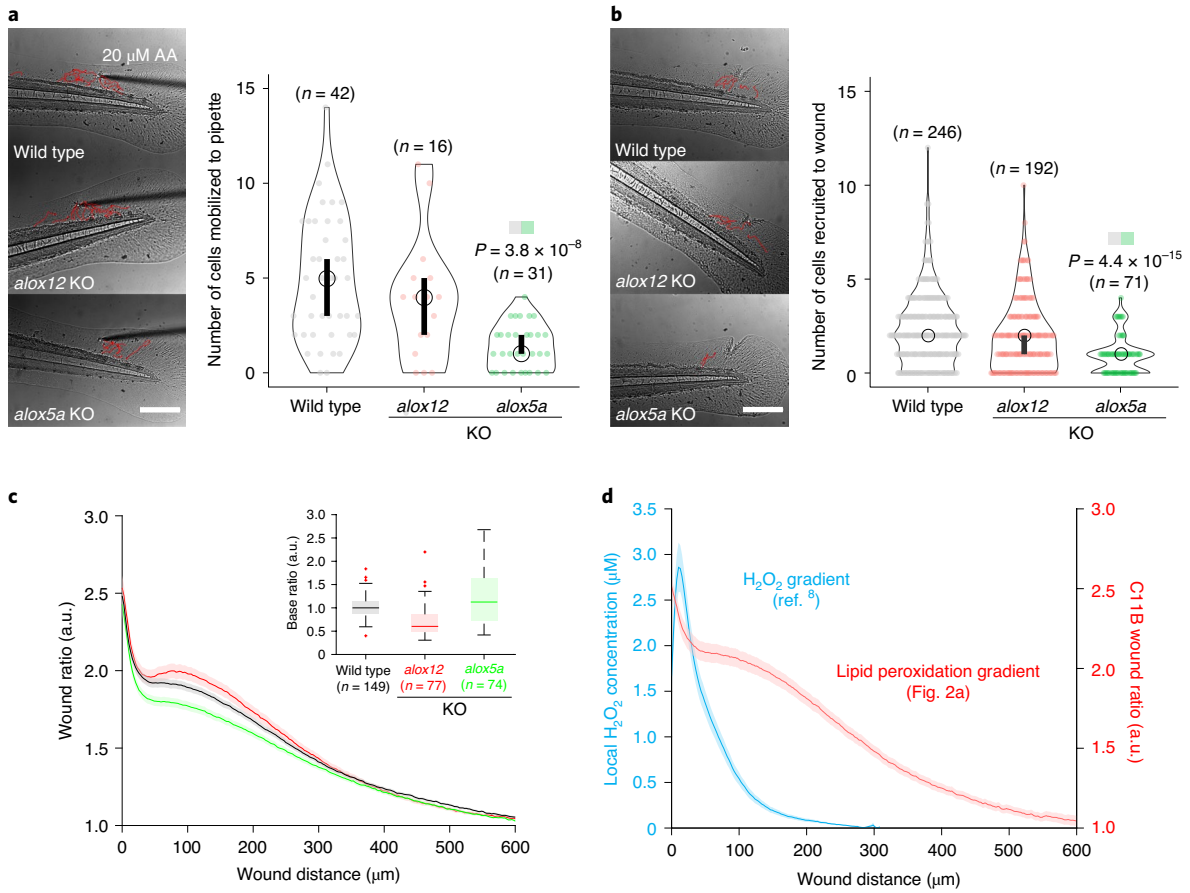

Fig. 4 | AA initiates wound detection through Alox5a. a,**b**, Left: representative images of wild-type, *alox12* knockout (KO) and *alox5a* KO tail fins patched with 20 μM AA at 20 min after patching (**a**) and wounded wild-type, *alox12* KO and *alox5a* KO tail fins at 40 min after injury (**b**). The red lines show the leukocyte tracks. Right: violin plots depicting the number of leukocytes per animal mobilized towards the pipette tip within 20 min (**a**) or the tail fin wound within 40 min after injury (**b**) for each genotype. For the violin plots in **a** and **b**: circles represent median values; bars represent 95% confidence intervals; statistical significance was determined by a two-sided, heteroscedastic Student's *t*-test for pairwise comparison of the indicated colour-coded samples; and the values in parentheses show the numbers of different animals. Data were aggregated from $n = 42$ (wild type in **a**), $n = 16$ (*alox12* KO in **a**), $n = 31$ (*alox5a* KO in **a**), $n = 246$ (wild type in **b**), $n = 192$ (*alox12* KO in **b**) and $n = 71$ (*alox5a* KO in **b**) biologically independent animal experiments. **c**, C11B ratios of wild-type, *alox12* KO and *alox5a* KO larvae ~15–30 min after tail fin amputation. The wound ratio (mean C11B ratio normalized to median baseline ratio ± s.e.m.) is plotted against the wound distance. Inset: box plots of baseline ratios normalized to controls. Central lines represent median values, whereas box edges represent the 25th and 75th percentiles. Whiskers show the most extreme, non-outlier data points. Outliers are shown by a plus sign. Data were aggregated from $n = 149$ (wild type), $n = 77$ (*alox12* KO) and $n = 74$ (*alox5a* KO) biologically independent animal experiments. **d**, Superposition of the calibrated wound H_2O_2 gradient (blue; published in Figs. 3d and 4 of Jelcic at al.[8]) and the lipid peroxidation gradient (red; *duox* MP; Fig. 2a) at ~15–30 min after tail fin tip amputation. Data are presented as mean values ± s.e.m. (shading). Scale bars, 200 μm (**a** and **b**).

comparison, we plotted the C11B green/red pixel ratios against wound distance (wound ratio) after internal normalization by the median baseline ratio (base ratio; insets). The wound ratio highlights wound-induced spatial changes in lipid peroxidation, whereas the base ratio reports on global lipid peroxidation shifts.

C11B imaging of live zebrafish larvae revealed extensive lipid peroxidation gradients extending ~0.5 mm from the wound margin into the unwounded tissue (Fig. 2a,b). Like the H_2O_2 gradient[2], and rapid leukocyte recruitment to AA and wounds, these patterns were inhibited by DPI and *duox* knockdown (Fig. 2a and Extended Data Fig. 1d,e). Unlike the wound H_2O_2 gradient[4,8], but just like leukocyte recruitment[4], lipid peroxidation gradients were completely suppressed by bath isotonicity (Fig. 2b), which prevents osmotic release of AA, and perhaps other PUFAs, by blocking mechanosensitive phospholipases, such as $cPla_2$[4,9]. Conversely, bath application of unsaturated fatty acids to unwounded larvae induced lipid peroxidation (Fig. 2c). The PUFAs linoleic acid (18:2), linolenic acid (18:3) and AA (20:4) caused more lipid peroxidation than single-unsaturated oleic acid (18:1). Saturated arachidic acid (20:0) induced no lipid peroxidation at all. Unsaturated fatty acids can activate NADPH oxidases[24]. Thereby, AA alone (for example, patched onto intact fins) seems to generate enough oxidative stress to drive its chemotactic conversion, even in the absence of other, wound-derived, ROS sources. Linoleic acid, which causes as much lipid peroxidation as AA, caused few leukocyte responses (Fig. 2d, Extended Data Fig. 4 and Supplementary Video 4). Again, this underlines that oxidative stress, at least at non-cytotoxic doses, ineffectively initiates inflammatory responses on its own. Instead, it acts through the AA pathway.

In the presence of excess thiols (for example, in vivo), the selenium-containing compound ebselen (Ebs) acts as a glutathione peroxidase mimetic. It antagonizes lipid peroxidation by reducing lipid hydroperoxides to lipid alcohols as opposed to radical scavenging[25]. Like *duox* knockdown, Ebs attenuated the lipid peroxidation gradient with little effect on baseline peroxidation levels (Fig. 3a). In contrast, the lipid radical scavenger and ferroptosis inhibitor

liproxstatin-1 (Lpx)[26] primarily affected baseline lipid peroxidation levels (Fig. 3b). This indicates that wound-induced peroxides initialize the gradient, and lipid radicals isometrically amplify the pre-pattern by perpetuating lipid auto-oxidation. Ebs, Lpx and the lipid radical scavenger α-TOC inhibited rapid leukocyte recruitment to wounds, suggesting that lipid peroxidation promotes wound detection (Fig. 3c,d and Supplementary Videos 5 and 6).

As discussed above, lipid peroxidation may exert its effects through redox regulation of lipoxygenases. Judging from messenger RNA (mRNA) and its 12-hydroxyeicosatetraenoic acid product levels, Alox12 is the predominant lipoxygenase in zebrafish larvae, followed by Alox5a [22,27]. Like their mammalian orthologues, zebrafish Alox5a and Alox12 generate 5(*S*)-HpETE and 12(*S*)-HpETE, respectively[27,28]. To test which, if any, of these enzymes is involved in wound detection, we generated CRISPR–Cas9 frameshift knockout mutants for both (Extended Data Figs. 2 and 3). Homozygous mutants grew to larval and adult stages without obvious developmental phenotypes. Leukocyte migration to microperfused AA and wounds, respectively, was strongly (72 and 61% on average; see the Source Data files for the respective figures) inhibited in *alox5a* mutant larvae, while overall leukocyte abundance in the tail fin was largely unaffected by the mutation (Fig. 4a,b, Supplementary Videos 7 and 8 and Extended Data Fig. 3e). *Alox5a* KO affected speed, persistence and directionality of leukocyte recruitment (Extended Data Fig. 4). In contrast, *alox12* mutant larvae showed only slightly (22 and 17% on average) attenuated leukocyte responses to microperfused AA or wounds, respectively. Relative to H_2O_2 inhibition by *duox* knockdown (Fig. 2a), lipoxygenase knockout had relatively little effect on lipid peroxidation gradients (Fig. 4c), suggesting that their pre-patterning occurs upstream of lipoxygenases and downstream of Duox. Compared with Lpx (Fig. 3b), *alox12* mutants only showed a moderate reduction of baseline lipid peroxidation (69 versus 29% on average). Together with the previously observed redox sensitivity of Alox5a product formation in vitro and in vivo[15,16,22], the above data collectively argue that lipid peroxidation gradients instruct wound detection through redox sensing by the Alox5a arm of the eicosanoid cascade. In humans, co-expression of $cPLA_2$, ALOX5 and DUOX1 occurs in the mucosal linings of the lower urinary tract[29], raising the possibility that this damage detection pathway is evolutionarily conserved.

It is conceivable that redox-sensitive wound chemoattractant production acts in concert with redox switches in leukocytes such as Lyn[3,7] to first initiate and later amplify rapid chemotaxis to zebrafish wounds. We cannot exclude that additional redox sensitivity exists downstream of Alox5a. For example, synthesis of the chemotactic AA metabolite 5-oxoETE, which we previously implicated in the early wound response[4], is putatively driven by the hypothetical enzyme 5-hydroxyeicosanoid dehydrogenase (5-HEDH), which requires $NADP^+$ as a cofactor[30]. Testing the contribution of 5-HEDH to wound redox sensing must await its genetic identification. Regardless, our work identifies eicosanoid metabolism as an instructive redox sensor of wound detection, with AA functioning akin to an alarmin[1]. Through redox activation of Alox5a, lipid peroxidation gradients may impinge on long-range production gradients of lipid chemoattractants (for example, of 5-oxoETE[4]) that directly guide distant leukocytes to wounds via conventional G protein-coupled receptor-mediated signalling. Likewise, there could be local Alox5a activation at the wound site and subsequent long-range diffusion of lipid chemoattractants, or any mixture of the above mechanisms, which may complement each other.

Currently, ROS signalling is mostly attributed to reversible cysteine oxidation of kinases and phosphatases, although physiological roles for lipid peroxidation are starting to emerge[31]. In zebrafish larvae, cytoplasmic antioxidants are predicted to confine H_2O_2-mediated cysteine oxidation to the immediate wound margin vicinity (<30 µm)[8]. Thus, it is difficult to envision how wound margin H_2O_2 can directly affect redox signalling in leukocytes 100–300 µm away. However, lipid peroxidation gradients reach much deeper into the tissue (Fig. 4d) and hence can act as a tissue-scale relay—potentially for both inflammatory cues and cell death (Extended Data Fig. 5).

Online content

Any methods, additional references, Nature Research reporting summaries, source data, extended data, supplementary information, acknowledgements, peer review information; details of author contributions and competing interests; and statements of data and code availability are available at https://doi.org/10.1038/s41556-020-0564-2.

Received: 28 January 2020; Accepted: 24 July 2020;
Published online: 31 August 2020

References

1. Huang, C. & Niethammer, P. Tissue damage signaling is a prerequisite for protective neutrophil recruitment to microbial infection in zebrafish. *Immunity* **48**, 1006–1013.e6 (2018).
2. Niethammer, P., Grabher, C., Look, A. T. & Mitchison, T. J. A tissue-scale gradient of hydrogen peroxide mediates rapid wound detection in zebrafish. *Nature* **459**, 996–999 (2009).
3. Yoo, S. K., Starnes, T. W., Deng, Q. & Huttenlocher, A. Lyn is a redox sensor that mediates leukocyte wound attraction in vivo. *Nature* **480**, 109–112 (2011).
4. Enyedi, B., Kala, S., Nikolich-Zugich, T. & Niethammer, P. Tissue damage detection by osmotic surveillance. *Nat. Cell Biol.* **15**, 1123–1130 (2013).
5. Enyedi, B. & Niethammer, P. Mechanisms of epithelial wound detection. *Trends Cell Biol.* **25**, 398–407 (2015).
6. Klyubin, I. V., Kirpichnikova, K. M. & Gamaley, I. A. Hydrogen peroxide-induced chemotaxis of mouse peritoneal neutrophils. *Eur. J. Cell Biol.* **70**, 347–351 (1996).
7. Evans, I. R., Rodrigues, F. S. L. M., Armitage, E. L. & Wood, W. Draper/CED-1 mediates an ancient damage response to control inflammatory blood cell migration in vivo. *Curr. Biol.* **25**, 1606–1612 (2015).
8. Jelcic, M., Enyedi, B., Xavier, J. B. & Niethammer, P. Image-based measurement of H_2O_2 reaction–diffusion in wounded zebrafish larvae. *Biophys. J.* **112**, 2011–2018 (2017).
9. Enyedi, B., Jelcic, M. & Niethammer, P. The cell nucleus serves as a mechanotransducer of tissue damage-induced inflammation. *Cell* **165**, 1160–1170 (2016).
10. Lämmermann, T. et al. Neutrophil swarms require LTB4 and integrins at sites of cell death in vivo. *Nature* **498**, 371–375 (2013).
11. Trede, N. S., Langenau, D. M., Traver, D., Look, A. T. & Zon, L. I. The use of zebrafish to understand immunity. *Immunity* **20**, 367–379 (2004).
12. Hammarström, S. et al. Increased concentrations of nonesterified arachidonic acid, 12*L*-hydroxy-5,8,10,14-eicosatetraenoic acid, prostaglandin E_2, and prostaglandin $F_{2\alpha}$ in epidermis of psoriasis. *Proc. Natl Acad. Sci. USA* **72**, 5130–5134 (1975).
13. Mathias, J. R. et al. Resolution of inflammation by retrograde chemotaxis of neutrophils in transgenic zebrafish. *J. Leukoc. Biol.* **80**, 1281–1288 (2006).
14. Gault, W. J., Enyedi, B. & Niethammer, P. Osmotic surveillance mediates rapid wound closure through nucleotide release. *J. Cell Biol.* **207**, 767–782 (2014).
15. Riendeau, D., Denis, D., Choo, L. Y. & Nathaniel, D. J. Stimulation of 5-lipoxygenase activity under conditions which promote lipid peroxidation. *Biochem. J.* **263**, 565–572 (1989).
16. Rouzer, C. A. & Samuelsson, B. The importance of hydroperoxide activation for the detection and assay of mammalian 5-lipoxygenase. *FEBS Lett.* **204**, 293–296 (1986).
17. Conrad, M. et al. Regulation of lipid peroxidation and ferroptosis in diverse species. *Genes Dev.* **32**, 602–619 (2018).
18. Linkermann, A. et al. Synchronized renal tubular cell death involves ferroptosis. *Proc. Natl Acad. Sci. USA* **111**, 16836–16841 (2014).
19. Kim, S. E. et al. Ultrasmall nanoparticles induce ferroptosis in nutrient-deprived cancer cells and suppress tumour growth. *Nat. Nanotechnol.* **11**, 977–985 (2016).
20. Riegman, M. et al. Ferroptosis occurs through an osmotic mechanism and propagates independently of cell rupture. *Nat. Cell Biol.* (in the press).
21. Yang, W. S. et al. Peroxidation of polyunsaturated fatty acids by lipoxygenases drives ferroptosis. *Proc. Natl Acad. Sci. USA* **113**, E4966–E4975 (2016).
22. Lebold, K. M. et al. Novel liquid chromatography–mass spectrometry method shows that vitamin E deficiency depletes arachidonic and docosahexaenoic acids in zebrafish (*Danio rerio*) embryos. *Redox Biol.* **2**, 105–113 (2013).
23. Pap, E. H. W. et al. Ratio-fluorescence microscopy of lipid oxidation in living cells using C11-BODIPY$^{581/591}$. *FEBS Lett.* **453**, 278–282 (1999).
24. Brash, A. R. Arachidonic acid as a bioactive molecule. *J. Clin. Invest.* **107**, 1339–1345 (2001).

25. Noguchi, N., Yoshida, Y., Kaneda, H., Yamamoto, Y. & Niki, E. Action of ebselen as an antioxidant against lipid peroxidation. *Biochem. Pharmacol.* **44**, 39–44 (1992).
26. Zilka, O. et al. On the mechanism of cytoprotection by ferrostatin-1 and liproxstatin-1 and the role of lipid peroxidation in ferroptotic cell death. *ACS Cent. Sci.* **3**, 232–243 (2017).
27. Adel, S., Heydeck, D., Kuhn, H. & Ufer, C. The lipoxygenase pathway in zebrafish. Expression and characterization of zebrafish ALOX5 and comparison with its human ortholog. *Biochim. Biophys. Acta* **1861**, 1–11 (2016).
28. Haas, U. et al. Targeted knock-down of a structurally atypical zebrafish 12S-lipoxygenase leads to severe impairment of embryonic development. *Proc. Natl Acad. Sci. USA* **108**, 20479–20484 (2011).
29. Uhlén, M. et al. A human protein atlas for normal and cancer tissues based on antibody proteomics. *Mol. Cell Proteom.* **4**, 1920–1932 (2005).
30. Erlemann, K.-R. et al. Airway epithelial cells synthesize the lipid mediator 5-oxo-ETE in response to oxidative stress. *Free Radic. Biol. Med.* **42**, 654–664 (2007).
31. Albadri, S. et al. Redox signaling via lipid peroxidation regulates retinal progenitor cell differentiation. *Dev. Cell* **50**, 73–89.e6 (2019).

Methods

General fish procedures. Adult wild-type and mutant Casper[32] zebrafish and larvae were maintained as previously described[33] and according to the institutional animal healthcare guidelines with the approval of the Memorial Sloan Kettering Cancer Center (MSKCC) Institutional Animal Care and Use Committee. For experiments at 2.5–4 d post-fertilization, larvae were anaesthetized in E3 medium (5 mM NaCl, 0.17 mM KCl, 0.33 mM $CaCl_2$ and 0.33 mM $MgSO_4$) containing 0.2 mg ml^{-1} ethyl 3-aminobenzoate methanesulfonate (Sigma–Aldrich; E10521). Sex was indeterminate at the stages of development that were used for the experiments described for this study.

Imaging leukocyte responses to wounds and micropipettes. To image leukocyte responses to wounds or micropipettes, anaesthetized larvae at 2.5–4 d post-fertilization were embedded in ~0.5 ml 1% isotonic low-melting agarose (GoldBio; A-204-100) in a glass-bottom dish (MatTek Corporation; P35G-1.5-20C). For the wounding experiments, the caudal tail fin was incised with a tungsten needle (Fine Science Tools; 10130-20) during agarose solidification. Transmitted light images were acquired at room temperature (~25 °C) using NIS-Elements (Nikon; version 64 bit 3.22.15 Build 738) on a Nikon Eclipse Ti microscope equipped with a 10×, plan-apochromat NA 0.45 air objective lens, and an Andor Clara charge-coupled device (CCD) camera. Multiple larvae were imaged in parallel using a motorized stage.

In some cases, leukocyte recruitment after pharmacological treatment was assessed. To this end, larvae were preincubated with 3 µM Ebs (Sigma–Aldrich; E3520), 20 µM Lpx (Sigma–Aldrich; SML1414) or 100 µM α-TOC (Sigma–Aldrich; 258024) in E3 medium for 30–60 min by bathing at 28 °C. Compound concentrations were maintained throughout the entire wounding/imaging experiment.

For the micropipette experiments, the agarose covering the tail fin was removed to allow tail fin patching. Glass capillaries (World Precision Instruments; TW100-3) were cut, polished and bent (~30°) using a microforge (Narishige; MF-900) to yield a tip diameter of ~10–20 µm. The micropipettes were filled with solutions using a syringe needle (World Precision Instruments; MF28G-5) and connected to a plastic syringe filled with the same solution. The following solutions were used: 5 or 20 µM AA (Sigma–Aldrich (A3611) or Cayman (90010)); 20 µM linoleic acid (Sigma–Aldrich; L1376) in E3 medium, either alone or in combination with 5 µM CHP (Invitrogen; included in the Image-iT Lipid Peroxidation Kit; C10445); or 50 µM DPI (Sigma–Aldrich; D2926). The micropipette was mounted onto the microscope using course and fine micromanipulators (Narishige; MN-4 and MMO-4) and lowered onto the caudal tail fin for attachment via mild negative pressure manually applied with the syringe. Transmitted light images were acquired every 15–30 s for 20 min at room temperature, as described above. Leukocytes that approached the pipette tip within 20 min of patching were counted as cells mobilized to the pipette.

Image-based measurement of lipid peroxidation. Anaesthetized larvae at 2.5–3 d post-fertilization were incubated in a solution of 10 µM C11B (Invitrogen; Image-iT Lipid Peroxidation Kit; C10445) in E3 medium for 30 min at 28 °C. Larvae were transferred to a glass-bottom dish and tail fin tips were amputated using a needle blade (Fine Science Tools; 10318-14) in the same C11B solution. Larvae were incubated for another 15 min at 28 °C, then washed three times with E3 medium. After mounting them in 1% low-melting agarose, C11B fluorescence was excited with an LED light source (Lumencor 7; Light Engine) with internal 549/15 and 475/28 bandpass filters, respectively, combined with a multispectral dichroic filter (Chroma; 89021bs). Emission of reduced C11B was sampled with a 632/60 bandpass filter (Chroma; ET632/60m) and emission of oxidized C11B was sampled with a 525/50 bandpass filter (Chroma; 525/50m). Transmitted light and C11B images were captured at room temperature using NIS-Elements Advanced Research software on a Nikon Eclipse Ti microscope equipped with a 10×, plan-apochromat NA 0.45 air objective lens and an Andor Clara CCD camera.

In some cases, the impact of pharmacological treatments on lipid peroxidation was assessed. To this end, larvae were co-incubated with 3 µM Ebs (Sigma–Aldrich; E3520), 20 µM Lpx (Sigma–Aldrich; SML1414) or 20–100 µM DPI, together with 10 µM C11B, in E3 medium for 30–60 min at 28 °C. C11B was washed off but compound concentrations were maintained throughout the imaging experiment.

Image analysis was primarily conducted in MATLAB (MathWorks; R2019b) using the custom scripts/functions ND2ratio, ND2SUM and Normalize WoundProfiles (https://github.com/niethamp/KatikaneniAndJelcic2020). Briefly, ND2 files were imported into MATLAB using the Bio-Formats toolbox for MATLAB (version 5.9; Open Microscopy Environment) function bfGetReader. In the transmitted light image, the wound margin and the notochord region were manually marked for the calculation of wound distances in pixels and for masking out the thick notochord region for quantitative C11B ratio analysis. Images were smoothed using a Gaussian filter if necessary (for example, at low camera binning). Modal background fluorescence was subtracted from the smoothed image. Green fluorescence emission was divided by red fluorescence emission. Thus, C11B ratios increase with lipid peroxidation. C11B ratios were calculated pixel by pixel together with their Euclidian distance from the wound margin. The median foreground C11B pixel ratio at 650–750 µm from the wound margin was defined as the baseline C11B ratio. All pixels of an animal (excluding the notochord region) were divided by this baseline ratio for normalization and plotted against their wound distance to yield the depicted normalized wound ratio profile. The baseline ratios (insets) for each experimental group were normalized by the median baseline ratio of all control animals.

To measure fatty acid-induced lipid peroxidation, uninjured and anaesthetized larvae at 2.5–3 d post-fertilization were embedded in ~0.5 ml 1% low-melting agarose in a glass-bottom dish. After solidification, the agarose surrounding the tail fins was removed with a needle blade to allow for better topical compound application. Larvae were preincubated for 60 min in 10 µM C11B in E3 medium at 28 °C. The C11B solution was replaced with carrier control (0.4% dimethyl sulfoxide (DMSO)) or 20 µM AA (Sigma–Aldrich; A3611), arachidic acid (Sigma–Aldrich; 10930), linolenic acid (Sigma–Aldrich; L2376), linoleic acid (Sigma–Aldrich; L1376) or oleic acid (Sigma–Aldrich; O1008) in E3 medium and incubated for 45 min at 28 °C. C11B images were acquired as described above. Image analysis was performed in MATLAB, essentially as detailed above, with the exception that a random polygonal region of the unwounded caudal tail fin (excluding the notochord) was selected from the transmitted light image for ratiometric C11B analysis.

Image-based measurement of tissue H_2O_2 production. Anaesthetized, unwounded larvae were embedded in 1% low-melting agarose in glass-bottom dishes. After solidification, the agarose covering the caudal tail fin part of the larvae was removed and 10 µM acetyl-pentafluorobenzene sulfonyl fluorescein (APSF; Calbiochem; 386794)[34] solution in E3 medium was added into the resulting well. Tail fins were exposed to the dye solution for ~40 min at room temperature before being washed three times with E3 medium supplemented with 5 µM CHP or DMSO carrier control. Either 5 µM CHP or DMSO (control) in E3 medium was then added to the wells. APSF fluorescence was excited with an LED light source with an internal 475/28 bandpass filter combined with a multispectral dichroic filter (Chroma; ET89021bs). APSF emission was sampled with a 525/50 bandpass filter (Chroma; ET525/50m). Transmitted light and APSF images were captured at room temperature using NIS-Elements on a Nikon Eclipse Ti microscope equipped with a 10×, plan-apochromat NA 0.45 air objective lens and an Andor Clara CCD camera with variable camera binning. Both control and CHP samples were acquired in parallel using a motorized stage with a double dish holder.

Analysis was conducted with the custom MATLAB script ND2Int (https://github.com/niethamp/KatikaneniAndJelcic2020). Briefly, ND2 files were imported using the Bio-Formats toolbox for MATLAB function bfGetReader. In the transmitted light image, a background region close to the fin and the tail fin region caudal to the notochord tip were manually marked for the calculation of background-corrected APSF signal in the caudal fin. Background-corrected APSF tail fin signals I_t at each time point t were normalized by calculating the relative fluorescence ΔI_t increase over the initial signal I_{t0} with $\Delta I_t = (I_t - I_{t0})/I_{t0}$.

Leukocyte-tracking analysis. Leukocytes were tracked in the ventral part of the caudal tail fin from transmitted light time-lapse videos using the MTrackJ[35] (version 1.5.1; imagescience.org) plugin of FIJI[36] (ImageJ version 1.5.2) by manually marking their position with the mouse cursor. Only clearly distinct positions were marked (that is, no clicking in place; marks were not placed in every frame). MDF files containing the tracking data were imported into MATLAB and processed with the custom scripts/functions AnalyzeMDF and AnalyzeMTrackJ (https://github.com/niethamp/KatikaneniAndJelcic2020) to obtain the average cell speed, persistence and directionality, as previously described[2,4], for animals with at least two tracks >50 µm. Such animals were categorized as responsive. Animals with fewer than two tracks >50 µm were categorized as non-responsive and excluded from the aggregated tracking analysis (Extended Data Fig. 4). The fraction of responsive versus non-responsive animals was calculated as a separate parameter and the results are represented as a pie chart in Extended Data Fig. 4. Statistical testing was conducted using the MATLAB fishertest function.

Sudan black staining of leukocytes. Leukocyte staining by Sudan black B (Sigma–Aldrich; 199664) was essentially performed as previously described[37] on euthanized wild-type or *alox5a*$^{-/-}$ larvae at 2.5–3 d post-fertilization.

Morpholino injection. One-cell-stage embryos were injected with 2.3 nl of 250–500 µM *duox* morpholino 1 (MO1: 5′- AAGCGTCACTTACTATAATG TTGGA-3′; Gene Tools) or misprime morpholino(MP: 5′-TCCCTTTTAGAA TTTACCTTGCCGA-3′; Gene Tools)[2], together with 200 µM *p53* morpholino (5′-ATGCTCAACTATAATGTTGGACATT-3′; Gene Tools)[38] diluted in water. *P53* morpholino co-injection with *duox* MO1/MP served to suppress potential pleiotropic morpholino-associated toxicity, as previously described[2,38].

To assess the efficacy of the injected morpholino, ~100 larvae (2 d post-fertilization) were dissociated in 500 µl TRIzol reagent (Invitrogen; 15596026) using RNase-free disposable pellet pestles (Fisherbrand; 12-141-364). Total RNA was extracted per the manufacturer's instructions. Contaminating DNA was removed using the TURBO DNA-free Kit (Invitrogen; AM1907). Knockdown was confirmed using the OneStep Ahead RT-PCR Kit (Qiagen; 220211) with the

following primers: *duox* forward (5′-ACACATGTGACTTCATATCCAG-3′) and *duox* reverse (5′-ATTATTAACTCATCCACATCCAG-3′).

Generation of *alox12*$^{-/-}$ zebrafish. Cas9 was cloned into the pCS2 vector to generate pCS2-Cas9. Capped mRNAs were transcribed using the mMESSAGE mMACHINE SP6 Transcription kit (Thermo Fisher Scientific; AM1340), DNase (Invitrogen; AM1907) treated and precipitated with lithium chloride. To generate templates for short guide RNA (sgRNA) transcription, gene-specific oligonucleotides against zebrafish *alox12* (ENSDARG00000069463) were designed using CHOPCHOP (https://chopchop.cbu.uib.no). An Sp6 consensus sequence was placed upstream of the targeting region of the *alox12* sgRNA for in vitro transcription of the sgRNA (Sp6: ATTTAGGTGACACTATA promoter sequence) and the 20-base target site of *alox12* (alox12: GGATCACTGGGCAGAAATAC) was annealed to a constant oligonucleotide encoding the reverse complement of the transactivating CRISPR RNA (tracrRNA) tail (5′–AAAAGCACCGACTCGGT GCCACTTTTTCAAGTTGATAACGGACTAGCCTTATTTTAACTTGCTATTT CTAGCTCTAAAAC–3′). The single-stranded DNA overhangs were filled in with T4 DNA polymerase (NEB; M0203) and the resulting sgRNA template was purified using QIAquick columns (Qiagen; 28115). sgRNAs were transcribed using the MEGAscript SP6 Transcription kit (Invitrogen; AM1330). All sgRNAs were DNase treated and precipitated with 3 M ammonium acetate/70% ethanol.

One-cell-stage Casper zebrafish zygotes were collected and the cytoplasm of the cell was injected with a single mix of 25 pg sgRNA and 100 pg Cas9 mRNA.

For sequencing, total RNA was isolated with TRIzol reagent from >50 F3 *alox12*$^{-/-}$ mutant zebrafish at 2.5–3 d post-fertilization. Each single mutant was reverse transcribed using the RevertAid First Strand cDNA Synthesis Kit (Thermo Fisher Scientific; K1622). The *alox12* gene was amplified with forward (5′-TTGAACAGAAACCTGATAAGGACA–3′) and reverse (5′-TGGCCACACAGATCACTTCT-3′) primers spanning intron/exon boundaries to ensure that mRNA was specifically amplified. The resulting amplicon was TA cloned with the StrataClone PCR Cloning kit (Aligent; 240205). Single colonies were isolated and Sanger sequenced.

Genomic DNA was isolated from the tail fins of adult F2 *alox12*$^{-/-}$ zebrafish. The HOT-SHOT genomic DNA isolation procedure was utilized. Briefly, 100 µl of 50 mM NaOH was added to each tail fin and incubated at 95 °C for 10 min. The genomic DNA was then placed on ice and 10 µl of 1 M Tris-HCl (pH 8.0) was added. The tube was spun down to remove debris and the resulting genomic DNA was used to amplify the region targeting *alox12* (see above). The resulting 164-base pair (bp) amplicon for wild-type and control samples was collected and sent to the MSKCC Integrated Genomics Core. The resulting amplicon had next-generation sequencing tails ligated onto the product and was sequenced on an Illumina next-generation sequencer at a respective read depth of >100,000 reads per sample. CRISPResso analysis was performed at the MSKCC Bioinformatics Core (http://crispresso.pinellolab.partners.org).

Generation of *alox5a*$^{-/-}$ zebrafish. An *alox5a* (ENSDARG00000057273) CRISPR RNA (crRNA), designed from the 20-base sequence 5′-TGGGTGCCGCCAAGTACTGA-3′, was selected from a pre-designed list of *alox5a*-targeting crRNAs generated by a propriety algorithm from Integrated DNA Technologies (IDT) and was ordered as an Alt-R CRISPR–Cas9 crRNA from IDT. The *alox5a* ALT-R crRNA and tracrRNA (IDT; 1072532) were solubilized in Nuclease-Free IDTE (pH 7.5) solution (IDT; 11-01-02-02) to final concentrations of 100 µM each. Solubilized *alox5a* crRNA and tracrRNA were mixed with Nuclease-Free Duplex Buffer (IDT; 11-01-03-01) to final concentrations of 3 µM each. The mixture was subsequently heated at 95 °C for 5 min, removed from the heat and allowed to cool to room temperature on the bench top to form the guide RNA (gRNA) solution. ALT-R S.p. Cas9 Nuclease (IDT; 1081058) was diluted to 1 mg ml^{-1} in solution containing 150 mM KCl and 20 mM HEPES (pH 7.5). Before injection, the Cas9-gRNA ribonucleoprotein complex was assembled by combining the gRNA and Cas9 protein solutions 1:1 (vol/vol) then incubating at 37 °C for 10 min and allowing it to cool to room temperature on the bench top. Subsequently, 2.3 nl of the Cas9-gRNA ribonucleoprotein complex solution was injected into the cytoplasm of one-cell-stage Casper zebrafish embryos, and injected F0 larvae were grown to sexual maturity (2–3 months post-fertilization). Individual F0 adults were crossed to wild-type Casper zebrafish and F1 progeny were collected. At 2.5–3 d post-fertilization, genomic DNA was isolated from four to six individual F1 larvae for genotyping. Briefly, euthanized larvae at 2.5–3 d post-fertilization were separately suspended in 100 µl of 50 mM NaOH and incubated at 95 °C for 10 min. Samples were then cooled on ice, neutralized with 10 µl of 1 M Tris-HCl (pH 8) and centrifuged at 16,000*g* to remove debris. The *alox5a* sequence of interest was PCR amplified from the genomic DNA samples with the following primers designed using CHOPCHOP: *alox5a* geno forward (5′-GCTGTAATCCAGTGGTCATCAA-3′) and *alox5a* geno reverse (5′-TGATCTCACTGGAGACTGGAGA-3′)[39]. Next, PCR products were incubated with the FastDigest ScaI (Thermo Fisher Scientific; FD0434) restriction enzyme for ~2 h at 37 °C, then samples were separated by agarose gel electrophoresis. F1 heterozygous larvae were identified by the presence of three double-stranded DNA products at ~1,102, 693 and 409 bp. The ~1,102-bp product signifies a mutant allele for which the ScaI restriction site has been destroyed as a result of a Cas9-induced double-strand break and subsequent DNA damage repair. F1 homozygous wild-type larvae were identified by the presence of only the 693- and 409-bp products, which are the result of complete digestion of the amplified wild-type allele by ScaI. An F0 *alox5a* knockout founder adult was identified by the presence of F1 heterozygous *alox5a* progeny. Once an F0 *alox5a* knockout founder adult was identified, the fish was once again crossed to a wild-type Casper. At 2.5–3 d post-fertilization, progeny tail fin tips were amputated and genomic DNA was isolated by suspending the tail fin tip in 20 µl of 50 mM NaOH then heating at 95 °C for 10 min. Samples were then cooled on ice, neutralized with 2 µl of 1 M Tris-HCl (pH 8) and centrifuged at 16,000*g* to remove debris. Genotyping was conducted by PCR amplification followed by ScaI digest. Heterozygous *alox5a* F1 larvae were identified and grown to sexual maturity. F1 adults were tail fin clipped to isolate genomic DNA and genotyped by PCR amplification and ScaI digest. The mutated alleles were sequenced by Sanger sequencing. F1 heterozygous male and female adults containing the frameshift mutation of interest (8-bp deletion; Extended Data Fig. 3) were crossed to generate F2 homozygous mutant *alox5a* progeny (*alox5a*$^{-/-}$).

Statistics and reproducibility. Sample sizes were not predetermined by statistical methods; rather, they were based on our previous experience with biological variability in this system. The results for each group plotted in the graphs typically represent data for $n=9$ or more biologically independent animal experiments, often aggregated from different experimental days (as indicated in the source data for the respective figures). For the micropipette experiments, we sequentially imaged animals, leading to lower experimental numbers compared with the wounding experiments, for which several wounded animals could be imaged in parallel using a motorized microscope stage. The group sizes in some of the leukocyte-tracking experiments are below $n=9$ (but at least $n=3$) because leukocytes in non-responsive animals could not be tracked (Extended Data Fig. 4). The experiments were not randomized and investigators were not blinded to allocation during the experiments and outcome assessment, with the following exceptions: parts of the wounding and patching experiments summarized in Fig. 4a,b were blinded by A.K. before the experiment and the results were analysed by P.N., to establish the principle mutant phenotypes at highest experimental rigour. Given its considerable logistic effort, blinding was later not consequently performed for the sake of increasing experimental throughput. During computational C11B and APSF image analysis in MATLAB, P.N. selected measurement regions based on the transmitted light images. Those images contained no result-relevant information, excluding the possibility of biased region picking based on lipid peroxidation signal intensity. Data were represented as dot plots, violin plots or box plots using the PlotsOfData[40] website (https://huygens.science.uva.nl/PlotsOfData/) or MATLAB. One dot in a graph represents $n=1$ biologically independent animal experiment (with a single larva). Numbers in parentheses represent the total n per group. Animals were never reused for different experiments. In the violin plots, the centre of an open circle indicates the median value and the vertical bar represents the 95% confidence interval. In the dot plots of Extended Data Fig. 4, the mean is denoted by a horizontal bar. Box plots were generated with the MATLAB boxplot function. Central marks indicate median values, whereas the bottom and top edges of the box indicate the 25th and 75th percentiles. Red crosses indicate outliers. Profile plots with shaded error regions were generated in MATLAB using the shadedErrorBar function (version 1.3.1; https://www.github.com/raacampbell/shadedErrorBar). The midline indicates the mean and the shaded region represents the s.e.m. *P* values for pairwise comparisons of samples were calculated using the Excel (Microsoft Office 365; Build 11929.20606) TTEST function (unpaired, two-tailed distribution; two-sample unequal variance). Two-tailed Fisher's exact tests were performed in MATLAB on the data shown in Extended Data Fig. 4.

The wave-like tissue degeneration phenomenon depicted in Extended Data Fig. 1c was observed twice from the total (including morphants and mutants) of 241 reported AA patching experiments (that is, at a frequency of ~1%).

Reporting Summary. Further information on research design is available in the Nature Research Reporting Summary linked to this article.

Data availability

All of the data supporting the findings of this study are available from the corresponding author upon reasonable request. Source data are provided with this paper.

Code availability

Custom MATLAB analysis code can be found at https://github.com/niethamp/KatikaneniAndJelcic2020.

References

32. White, R. M. et al. Transparent adult zebrafish as a tool for in vivo transplantation analysis. *Cell Stem Cell* **2**, 183–189 (2008).
33. Nüsslein-Volhard, C. & Dahm, R. *Zebrafish: A Practical Approach* 303 (Oxford Univ. Press, 2002).
34. Maeda, H. et al. Fluorescent probes for hydrogen peroxide based on a non-oxidative mechanism. *Angew. Chem. Int. Ed. Engl.* **43**, 2389–2391 (2004).

35. Meijering, E., Dzyubachyk, O. & Smal, I. Methods for cell and particle tracking. *Meth. Enzymol.* **504**, 183–200 (2012).
36. Schindelin, J. et al. Fiji: an open-source platform for biological-image analysis. *Nat. Methods* **9**, 676–682 (2012).
37. Rosowski, E. E. et al. Macrophages inhibit *Aspergillus fumigatus* germination and neutrophil-mediated fungal killing. *PLoS Pathog.* **14**, e1007229 (2018).
38. Robu, M. E. et al. p53 activation by knockdown technologies. *PLoS Genet.* **3**, e78 (2007).
39. Labun, K., Montague, T. G., Gagnon, J. A., Thyme, S. B. & Valen, E. CHOPCHOP v2: a web tool for the next generation of CRISPR genome engineering. *Nucleic Acids Res.* **44**, W272–W276 (2016).
40. Postma, M. & Goedhart, J. PlotsOfData—a web app for visualizing data together with their summaries. *PLoS Biol.* **17**, e3000202 (2019).

Acknowledgements

This research was supported by the NIH/NIGMS grants R01GM099970 and R01GM127356 to P.N. and the MSKCC Functional Genomics Initiative, and in part through NIH/NCI Cancer Center Support grant P30CA008748. We thank the Integrated Genomics Operation Core and Bioinformatics Core at MSKCC for assistance.

Author contributions

P.N. conceived of the study and its experiments and conducted them with A.K. M.J. generated and characterized the *alox5a* mutant fish. G.F.G. generated and characterized the *alox12* mutant fish. Y.M. performed Sudan black staining of leukocytes. M.O. provided general advice on ferroptotic mechanisms. P.N. analysed the data, prepared the figures and wrote the paper, together with A.K., M.J., G.F.G. and M.O.

Competing interests

The authors declare no competing interests.

Additional information

Extended data Extended data is available for this paper at https://doi.org/10.1038/s41556-020-0564-2.

Supplementary information Supplementary information is available for this paper at https://doi.org/10.1038/s41556-020-0564-2.

Correspondence and requests for materials should be addressed to P.N.

Reprints and permissions information is available at www.nature.com/reprints.

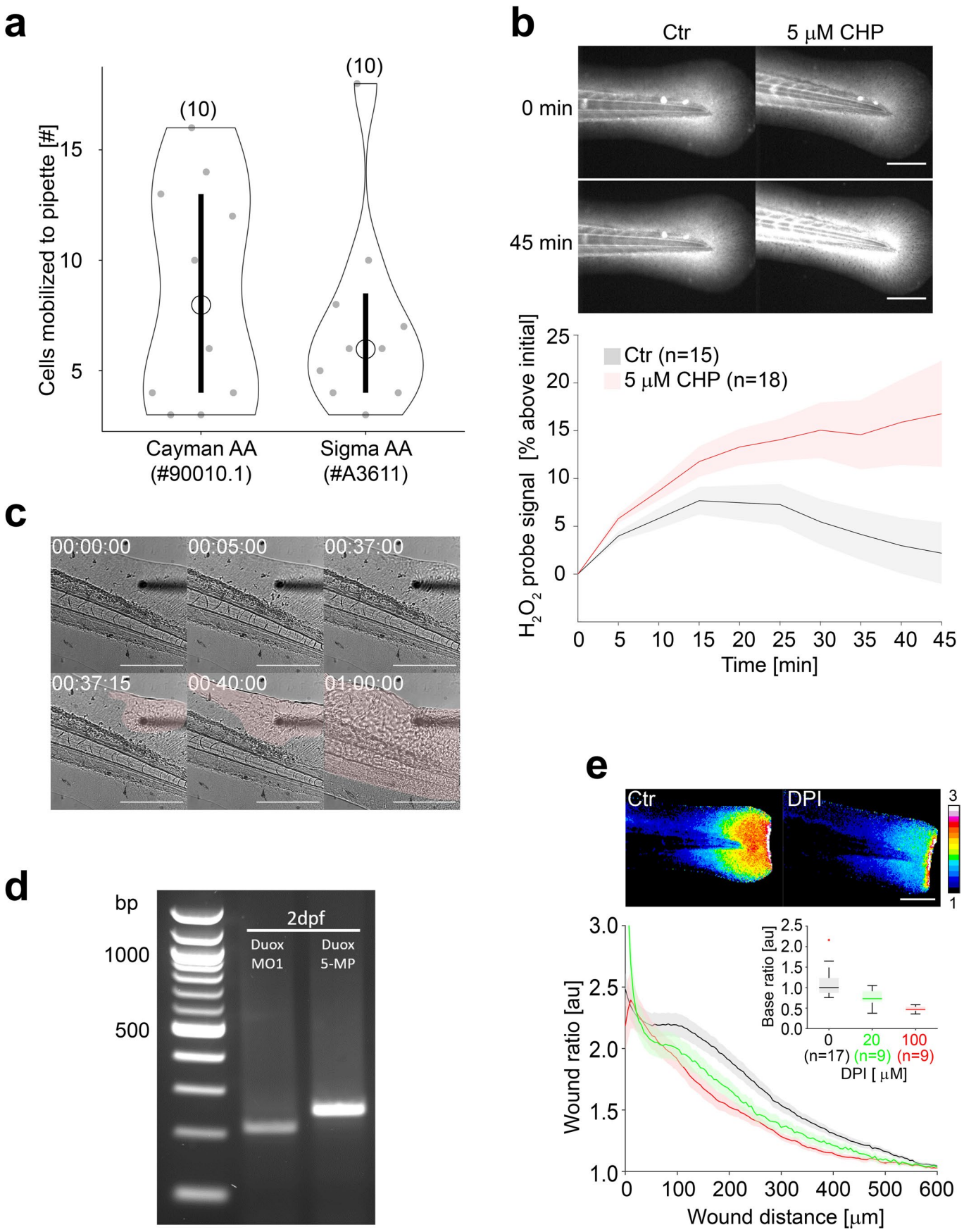

Extended Data Fig. 1 | See next page for caption.

Extended Data Fig. 1 | Additional data supporting Figs. 1 and 2. a, Leukocyte mobilization to different AA preparations. Circles, median. Bars, 95% confidence interval. Data aggregated from n=10 (Cayman AA), and n=10 (Sigma AA) biologically independent animal experiments. No significant difference (p=0.51) detected between groups by two-sided, heteroscedastic Student's t-test. **b**, CHP stimulates H_2O_2. Zebrafish tail fins of wild type larvae were loaded with the H_2O_2 sensor dye acetyl-pentafluorobenzene sulphonyl fluorescein, and then exposed to 5 μM CHP or DMSO control (Ctr). Top panel, representative dye emission images at 0 min and 45 min after CHP exposure. Lower panel, plots (mean ± SEM) of normalized dye fluorescence over 45 min after CHP exposure. Data aggregated from n=15 (Ctr), and n=18 (CHP) biologically independent animal experiments **c**, Time-lapse montage of a wave-like tissue degeneration emerging from an AA (20 μM) microperfusion patch site. Pink shade highlights the affected region. Time, hh:mm:ss. Images representative of the 2 out of 241 biologically independent animal experiments with observable waves. **d**, Confirmation of *duox* knockdown by RT-PCR in 2 dpf embryos. Representative for three independent analyses. **e**, C11B-imaging of control larvae (Ctr) and larvae treated with 20 μM or 100 μM DPI ~15-30 min after tail fin tip amputation. Upper panel: Representative C11B ratio images. Lower panel: Wound ratio, mean C11B ratio normalized to median baseline ratio ± SEM plotted against wound distance. Inset, boxplots of baseline ratios normalized to control. Central mark, median. Box edges, 25^{th}/75^{th} percentiles. Whiskers, most extreme, non-outlier data points. +, outliers. Data aggregated from n=17 (Ctr, 0 μM DPI), n=9 (20 μM DPI), and n=9 (100 μM DPI) biologically independent animal experiments. Parentheses, number of different animals. Scale bar, 200 μm. Statistical source data can be found at Source data Extended Data Figure 1.

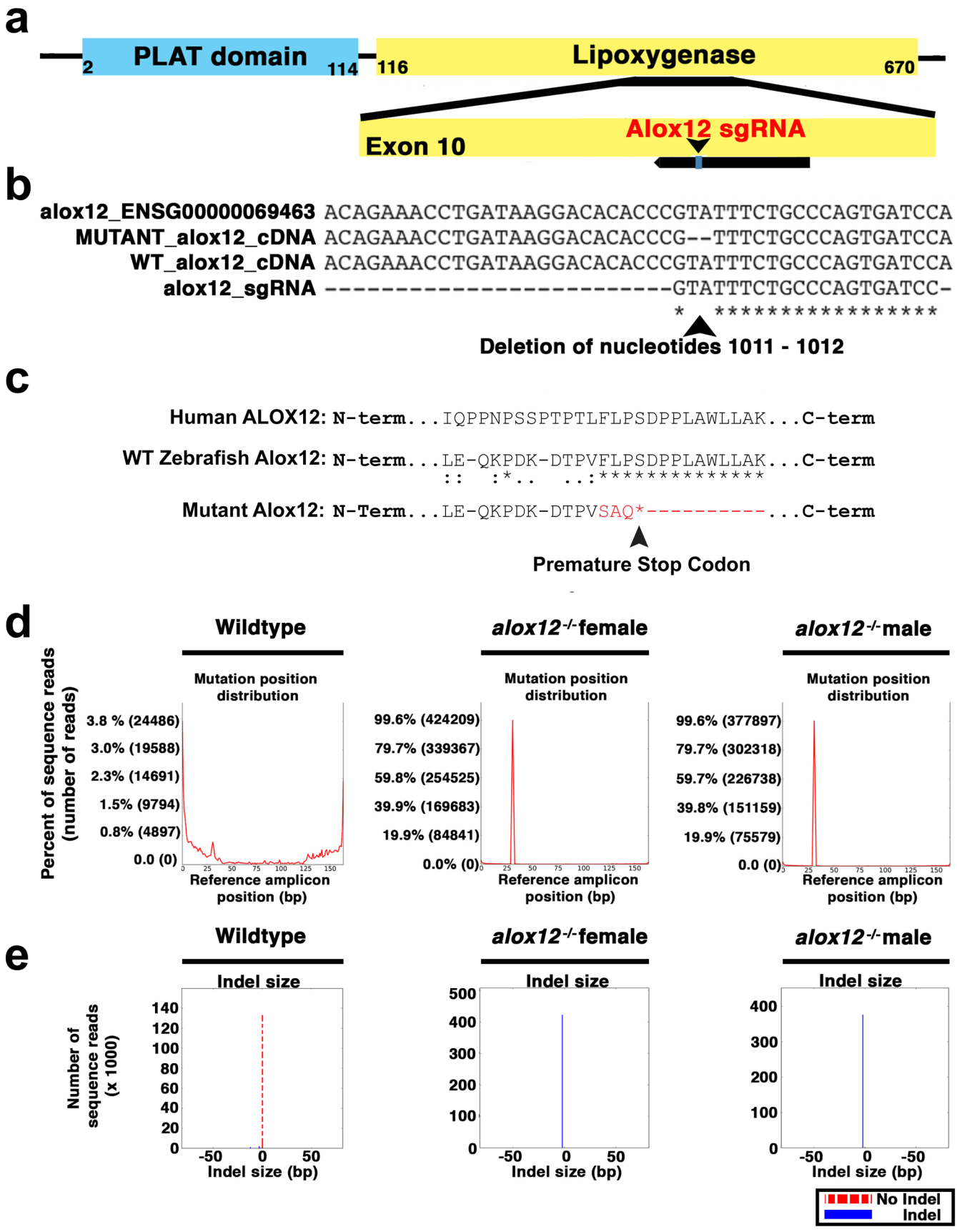

Extended Data Fig. 2 | See next page for caption.

Extended Data Fig. 2 | Characterization of the *alox12* KO mutant. a, Schematic representation of the protein domains of zebrafish 12-lipxoygenase (Alox12). The lipoxygenase domain of Alox12 responsible for enzymatic function was targeted with a short guide RNA (sgRNA). **b**, Sanger sequence analysis of cDNA identified a two-base pair deletion at nucleotide position 1011-1012 within exon 10 of *alox12*. **c**, The targeted region of the lipoxygenase domain of zebrafish Alox12 is well conserved compared to human ALOX12. The frameshift mutant *alox12* allele contains a premature stop codon in the coding sequence. Asterisks, fully conserved residues. Colons, conservation of strongly similar residues. Periods, conservation of weakly similar residues. **d**, Next-Gen Sequencing and CRISPResso analysis of the amplicon containing the sgRNA cut site was performed on genomic DNA from tail fin clips of F2 adult *alox12*-targeted zebrafish. *Alox12*-targeted F2 male and female zebrafish exhibited a 2 bp mutation positioned at the proposed sgRNA cut site in greater than 99% of sequence reads over a depth of more than 300 and 400 thousand reads, respectively. Wild type zebrafish displayed background sequence abnormalities below 1% in more than 140 thousand total reads. **e**, CRISPResso analysis of F2 male and female zebrafish targeted with the sgRNA against *alox12* identifies a single 2 bp indel. An indel is denoted by a blue solid bar and no indel is represented by a red dashed bar. Wildtype zebrafish display no indels in most of the sequence reads.

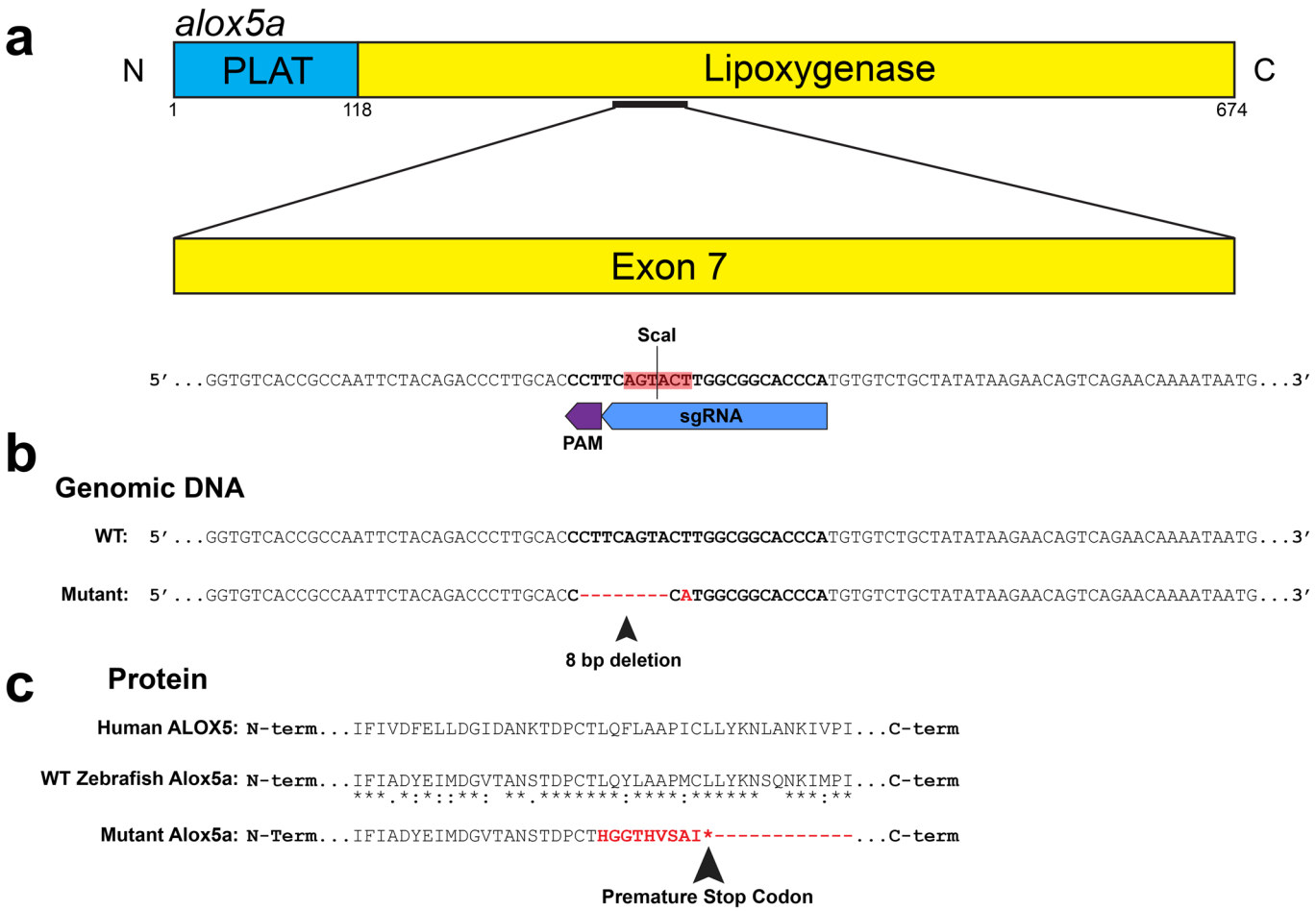

Extended Data Fig. 3 | See next page for caption.

Extended Data Fig. 3 | Characterization of the *alox5a* KO mutant. a, Schematic representation of zebrafish Alox5a. A single guide RNA (sgRNA) was designed to target *alox5a* for gene disruption within the lipoxygenase domain at exon 7 (bold text). Successful target disruption is predicted to occur at a ScaI restriction enzyme recognition site (AGTˆACT) (highlighted red text) within the genomic DNA (gDNA) sequence, potentially destroying the sequence upon DNA repair. **b**, *alox5a* wild type and knockout mutant alleles. The mutant *alox5a* allele contains an 8-base pair (bp) deletion resulting in a frameshift and the destruction of the ScaI restriction enzyme recognition site. Red text, mutant *alox5a* sequence that differs from the wild type sequence. **c**, The targeted region of the lipoxygenase domain of zebrafish Alox5a is highly conserved compared to human ALOX5. The mutant *alox5a* allele contains a premature stop codon in the coding sequence, resulting in a truncated Alox5a. Asterisks, fully conserved residues. Colons, conservation of strongly similar residues. Periods, conservation of weakly similar residues. Red text, mutant Alox5a sequence that differs from the wild type sequence. **d**, Heterozygous *alox5a* larvae were crossed and gDNA from isolated progeny was PCR amplified, ScaI-digested, and analyzed by agarose gel electrophoresis for genotyping. PCR product from the wild type *alox5a* allele is cleaved into two smaller products upon incubation with ScaI (409 and 693 bp products). The mutant *alox5a* allele is not cleaved by ScaI (1094 bp product only). Heterozygotes are identified by the combined presence of a cleaved wild type allele and non-cleaved mutant allele (409, 693, and 1094 bp products). Representative of three independent analyses. **e**, Sudan black-stained neutrophils in the tail region of zebrafish larvae at 2.5-3 days post fertilization. Shown are three representative animals from a total of 20 different larvae stained per genotype. Scale bar, 200 μm.

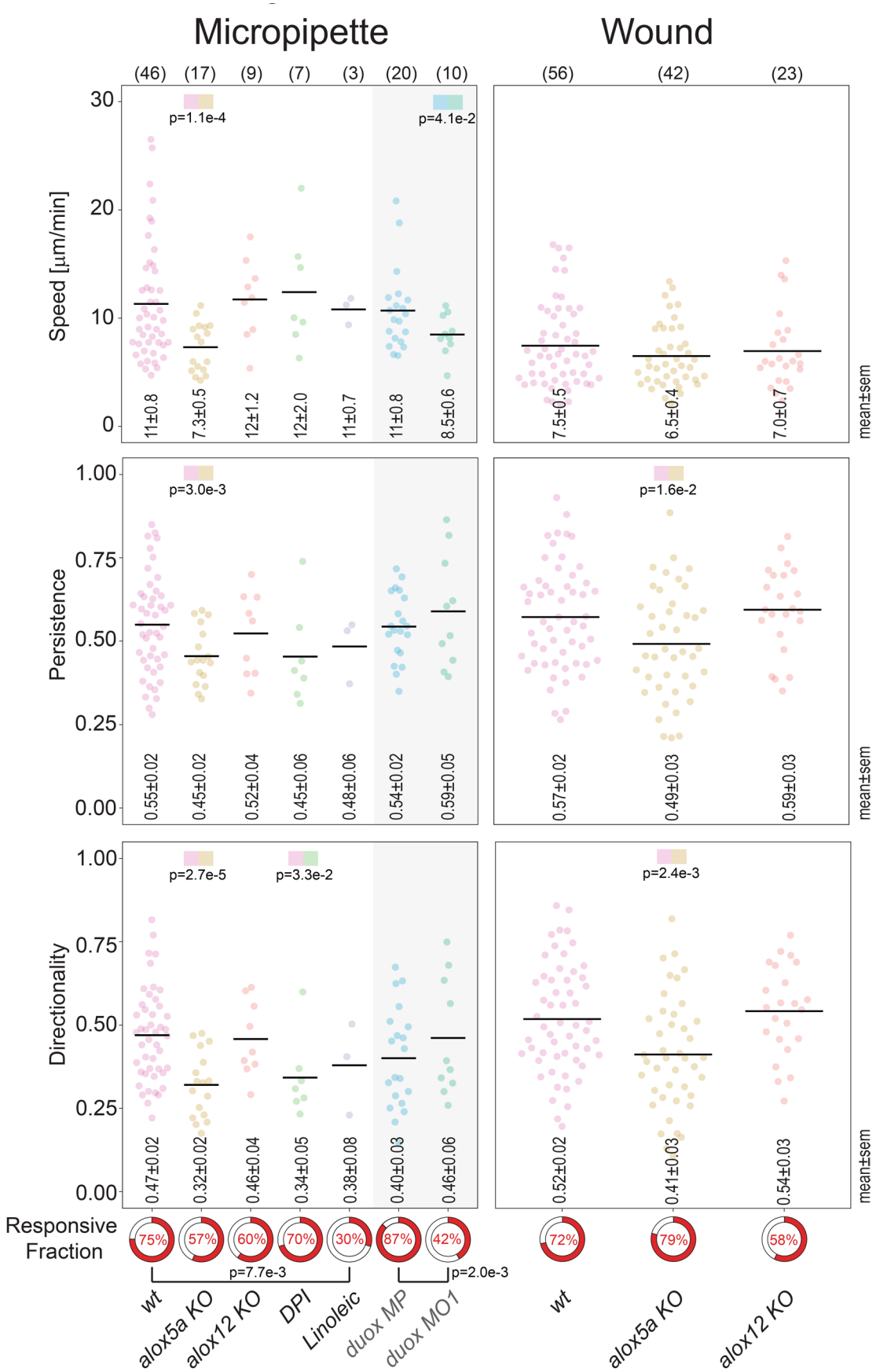

Extended Data Fig. 4 | See next page for caption.

Extended Data Fig. 4 | Aggregated leukocyte tracking analysis. Left panels: leukocyte speed, migration persistence, directionality, and responsiveness towards microperfused 20 μM AA tracked over 20 min after patching. Right panels: leukocyte speed, migration persistence, directionality, and responsiveness towards a tail fin wound tracked over 40 min after tail fin injury. Leukocyte speed, migration persistence, directionality was calculated as previously described (see Methods). The *Responsive Fractions* (red color, pie charts) denote the fractions of animals for which at least two tracks > 50 μm could be reliably measured in the caudal tail fin below the notochord line. Tracking data are only aggregated for *responsive* animals. Only clearly distinct positions were marked for tracking; stationary leukocytes were not tracked. The tracking analysis was performed on the time lapse data underlying Fig. 1c, 2d and 4a, b, and an additional AA/DPI pipette experiment, in which leukocyte migration to a micropipette filled with 20 μM AA + 50 μM DPI (DPI, green dots) was tracked. Gray shaded region, *duox* MO1 morphants were compared to *duox* MP animals instead of *wild type* animals, as both samples are also co-morphants for *p53* (see Methods). Horizontal bars, mean. Data aggregated from n=46 (*wt*, Micropipette), n=17 (*alox5a* KO, Micropipette), and n=9 (*alox12* KO, Micropipette), n=7 (DPI, Micropipette), n=3 (Linoleic, Micropipette), n=20 (*duox* MP, Micropipette), n=10 (*duox* MO1, Micropipette), n=56 (*wt*, Wound), n=42 (*alox5a* KO, Wound), and n=23 (*alox12* KO, Wound) biologically independent animal experiments. P-values with color code, two-sided, heteroscedastic Student's t-test for pairwise comparison of the indicated color-coded samples. P-value near brackets, two-tailed Fisher's exact test between *Responsive Fractions* indicated by brackets. Parentheses, number of different animals. Statistical source data can be found at Source data Extended Data Figure 4.

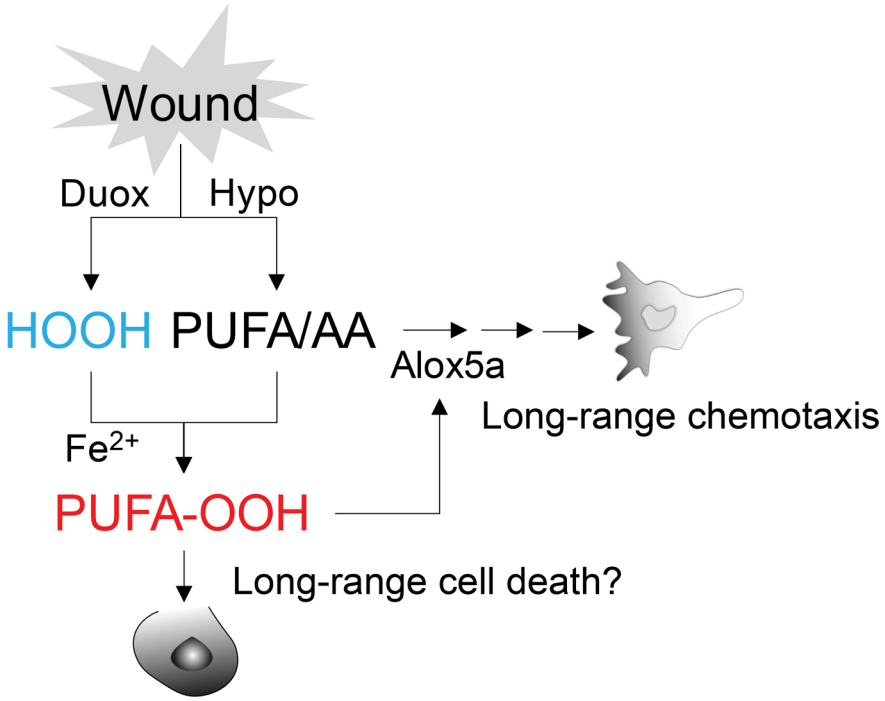

Extended Data Fig. 5 | Cartoon scheme of proposed mechanism. Wounding activates Duox to produce H_2O_2 and causes hypotonic (Hypo) shock, which leads to release of PUFAs (including AA). H_2O_2 reacts with Fe^{2+} to generate HO• by Fenton chemistry. HO• reacts with PUFAs/AA to generate long-chain lipid ROS (PUFA-OO•, PUFA-OOH) that further promote lipid peroxidation, and activate Alox5a to produce leukocyte chemoattractants. If lipid peroxidation slips out of control, it may cause cell death.

nature research

Corresponding author(s): Philipp Niethammer

Last updated by author(s): Jul 14, 2020

Reporting Summary

Nature Research wishes to improve the reproducibility of the work that we publish. This form provides structure for consistency and transparency in reporting. For further information on Nature Research policies, see Authors & Referees and the Editorial Policy Checklist.

Statistics

For all statistical analyses, confirm that the following items are present in the figure legend, table legend, main text, or Methods section.

n/a	Confirmed	
☐	☒	The exact sample size (*n*) for each experimental group/condition, given as a discrete number and unit of measurement
☐	☒	A statement on whether measurements were taken from distinct samples or whether the same sample was measured repeatedly
☐	☒	The statistical test(s) used AND whether they are one- or two-sided *Only common tests should be described solely by name; describe more complex techniques in the Methods section.*
☒	☐	A description of all covariates tested
☐	☒	A description of any assumptions or corrections, such as tests of normality and adjustment for multiple comparisons
☐	☒	A full description of the statistical parameters including central tendency (e.g. means) or other basic estimates (e.g. regression coefficient) AND variation (e.g. standard deviation) or associated estimates of uncertainty (e.g. confidence intervals)
☐	☒	For null hypothesis testing, the test statistic (e.g. *F*, *t*, *r*) with confidence intervals, effect sizes, degrees of freedom and *P* value noted *Give P values as exact values whenever suitable.*
☒	☐	For Bayesian analysis, information on the choice of priors and Markov chain Monte Carlo settings
☒	☐	For hierarchical and complex designs, identification of the appropriate level for tests and full reporting of outcomes
☒	☐	Estimates of effect sizes (e.g. Cohen's *d*, Pearson's *r*), indicating how they were calculated

Our web collection on statistics for biologists contains articles on many of the points above.

Software and code

Policy information about availability of computer code

Data collection	NIS-Elements AR 3.2 64 bit (Nikon) Bioformats Toolbox for MATLAB v5.9 (OME) including bfGetReader function
Data analysis	MATLAB R2019b (MathWorks) including boxplot and fishertest function. FIJI (ImageJ v1.5.2) MTrackJ for ImageJ (v1.5.1, imagescience.org) PlotsOfData (https://huygens.science.uva.nl/PlotsOfData/) shadedErrorBar (v1.3.1, https://www.github.com/raacampbell/shadedErrorBar) for MATLAB Excel (Microsoft Office 365, Build 11929.20606) including TTEST

For manuscripts utilizing custom algorithms or software that are central to the research but not yet described in published literature, software must be made available to editors/reviewers. We strongly encourage code deposition in a community repository (e.g. GitHub). See the Nature Research guidelines for submitting code & software for further information.

Data

Policy information about availability of data

All manuscripts must include a data availability statement. This statement should provide the following information, where applicable:

- Accession codes, unique identifiers, or web links for publicly available datasets
- A list of figures that have associated raw data
- A description of any restrictions on data availability

Numerical source data underlying Figure 1, 2, 3, 4 and Extended Data Figure 1, 4 are provided with this paper. All other data supporting the findings of this study are available from the corresponding author upon reasonable request.
Code availability: Custom MATLAB analysis code can be found on https://github.com/niethamp/KatikaneniAndJelcic2020.

Field-specific reporting

Please select the one below that is the best fit for your research. If you are not sure, read the appropriate sections before making your selection.

☒ Life sciences ☐ Behavioural & social sciences ☐ Ecological, evolutionary & environmental sciences

For a reference copy of the document with all sections, see nature.com/documents/nr-reporting-summary-flat.pdf

Life sciences study design

All studies must disclose on these points even when the disclosure is negative.

Sample size	Sample sizes were not predetermined by statistical methods and based on our previous experience with biological variability in this system. Each group plotted in the graphs typically contains n=9 or more biologically independent animal experiments often aggregated from different experimental days (as indicated in the Source data for the respective figures). For micropipette experiments, we sequentially imaged animals leading to lower experimental numbers as compared to wounding experiments, where several wounded animals could be imaged in parallel using a motorized microscope stage. Note that group sizes in some of the leukocyte tracking experiments are below n=9 (but at least n=3), because leukocytes in non-responsive animals were not tracked (Extended Data Figure 4).
Data exclusions	Data exclusion criteria were preestablished based on our previous experience with these assays. Leukocyte recruitment experiments: Animals inadvertently injured more than one time were excluded from the analysis. If wounds were too small (~<30 um incision length), animals were excluded from analysis. If the micropipette was not firmly attached to the animal (e.g., indicated by sample moving underneath pipette), animals were excluded from analysis. If sample movements were obscuring the data, or if the focus was too much off to accurately count leukocytes, samples were excluded from analysis. If leukocytes were already at the wound (or ~<50 um distance) at t=0 of the time lapse, these leukocytes were not included in the count. For tracking analysis: If animals showed less than two leukocyte tracks > 50 um they were excluded from the cumulative analysis. C11B measurements: Animals were excluded if they were out of focus. Animals were excluded if overexposed, or if signal level was too low/noisy. The global background could not be accurately determined (e.g., if more than one animal were within one field of view, or if background was too inhomogeneous). In the Base Ratio insets, outliers are marked according to the default MATLAB boxplot settings by red crosses.
Replication	To ensure reproducibility, all data figures used to support our main conclusions sample data from at least 3 and up to 246 biologically independent animal experiments, often aggregated from different experimental days as indicated in the respective Source data files. Orthogonal genetic/pharmacologic perturbations (e.g., duox MO & DPI, Ebselen & Liproxstatin-1/alpha-tocopherol) or experimental designs (micropipette & tail fin wounding) were used for cross-validation. The tissue degeneration wave to AA-patching (Extended Data Figure 1c) was observed in two independent animals (out of ~200) as indicated in the respective legend.
Randomization	For drug treatments, animals were picked randomly out of a pool of animals with the same genotype (morphant type). For assuring the central Alox5a leukocyte recruitment phenotype, leukocyte abundance was tested as potential covariate, and found to be unchanged.
Blinding	Investigators were not blinded to allocation during experiments and outcome assessment with the following exceptions: Part of the wounding experiments summarized in Figure 4a and 4b were blinded by AK prior to experiment and analysis by PN to establish the principle mutant phenotypes at highest experimental rigor. Given its considerable logistic effort, blinding was not performed in all experiments for the sake of increasing experimental throughput. During computational C11B image analysis in MATLAB, PN was selecting measurement regions based on the transmitted light images, which contained no result-relevant information (i.e., C11B emission intensity), excluding the possibility of biased region-picking based on lipid peroxidation signal intensity.

Reporting for specific materials, systems and methods

We require information from authors about some types of materials, experimental systems and methods used in many studies. Here, indicate whether each material, system or method listed is relevant to your study. If you are not sure if a list item applies to your research, read the appropriate section before selecting a response.

Materials & experimental systems

n/a	Involved in the study
☒	☐ Antibodies
☒	☐ Eukaryotic cell lines
☒	☐ Palaeontology
☐	☒ Animals and other organisms
☒	☐ Human research participants
☒	☐ Clinical data

Methods

n/a	Involved in the study
☒	☐ ChIP-seq
☒	☐ Flow cytometry
☒	☐ MRI-based neuroimaging

Animals and other organisms

Policy information about studies involving animals; ARRIVE guidelines recommended for reporting animal research

Laboratory animals	Adult (for embryo rearing) and larval (up to 4 days post fertilization for experiments) Casper zebrafish (danio rerio). Sex was indeterminate at the stages of development (2.5-4 dpf) that were used in all experiments with zebrafish larvae.
Wild animals	no wild animals were used in this study
Field-collected samples	no field-collected samples were used in this study
Ethics oversight	Institutional Animal Care and Use Committee of Memorial Sloan Kettering Cancer Center (MSKCC)

Note that full information on the approval of the study protocol must also be provided in the manuscript.